

Chiral extrapolation of g_A with explicit $\Delta(1232)$ degrees of freedom

M. Procura, B. U. Musch, T. R. Hemmert and W. Weise

*Physik-Department, Theoretische Physik
Technische Universität München, D-85747 Garching, Germany*

Abstract

An updated and extended analysis of the quark mass dependence of the nucleon's axial vector coupling constant g_A is presented in comparison with state-of-the-art lattice QCD results. Special emphasis is placed on the role of the $\Delta(1232)$ isobar. It is pointed out that standard chiral perturbation theory of the pion-nucleon system at order p^4 fails to provide an interpolation between the lattice data and the physical point. In contrast, a version of chiral effective field theory with explicit inclusion of the $\Delta(1232)$ proves to be successful. Detailed error analysis and convergence tests are performed. Integrating out the $\Delta(1232)$ as an explicit degree of freedom introduces uncontrolled errors for pion masses $m_\pi \gtrsim 300$ MeV.

1 Introduction

The axial-vector coupling constant g_A of the nucleon represents a benchmark test of our ability to extract hadron properties from the QCD Lagrangian. Its empirical value is accurately determined from neutron β -decay [1]: $g_A = 1.267 \pm 0.003$. On the other side, both lattice QCD calculations [2, 3, 4] and chiral effective field theories [5, 6, 7] are making progress in describing the quark mass dependence of this nucleon property.

The present paper updates and extends our previous study in Ref. [6] about chiral extrapolations for g_A , in the continuum and infinite volume limit. We refer to [8, 4, 9] for chiral perturbation theory analyses of the effects due to the finite spatial extent of the lattice simulation volume [10]. In Ref. [6] we compared two different two-flavor, non-relativistic chiral effective field theories at leading-one-loop level: Heavy Baryon Chiral Perturbation Theory (HB χ PT), with pions and nucleons as active degrees of freedom, and the so-called Small Scale Expansion (SSE), which includes the $\Delta(1232)$ explicitly. Treating the $\Delta(1232)$ as an explicit degree of freedom turned out to be crucial in order to obtain a consistent extrapolation of available lattice data down to the region of small quark masses.

The important role played by the $\Delta(1232)$ in the physics behind g_A does not come as a surprise. It has in fact been known for decades that the Δ -dominance of P -wave pion-nucleon scattering, or equivalently, the strong spin-isospin polarizability of the nucleon, has its pronounced impact on matrix elements of the axial current in the nucleon ground state. The Adler-Weisberger sum rule is a prominent example illustrating this connection. Extended versions of chiral effective field theories, such as SSE, have been designed to incorporate these well established features.

A surprising outcome of lattice QCD results for g_A is their weak dependence on the quark mass. This suggests a subtle balance between contributions from the different degrees of freedom involved. In Section 2 we first demonstrate that no interpolation between physical point and state-of-the-art lattice results is possible, with parameters consistent with hadron phenomenology, if we use standard chiral perturbation theory with only pions and nucleons up to next-to-leading-one-loop order. This observation holds both for the non-relativistic and infrared regularized, manifestly covariant scheme [11]. Section 3 recalls the Adler-Weisberger sum rule and outlines the importance of the $\Delta(1232)$ for g_A in a simple schematic model. In Section 4.1 we present a detailed statistical analysis showing that the leading-one-loop SSE expression with explicit $\Delta(1232)$ worked out in Ref. [6] does lead to successful interpolations with recent lattice results even for relatively large values of m_π . Remarkably, the outcome of our fits turns out to be consistent with available phenomenological information about the low-energy couplings involved. In Section 4.2 we explore the mapping between expressions worked out with and without explicit $\Delta(1232)$ by examining the separate contributions of different powers of m_π in the expanded SSE result. Conclusions are drawn in Section 5.

Part of this study has been anticipated in several conference proceedings, see Refs. [12, 13, 14].

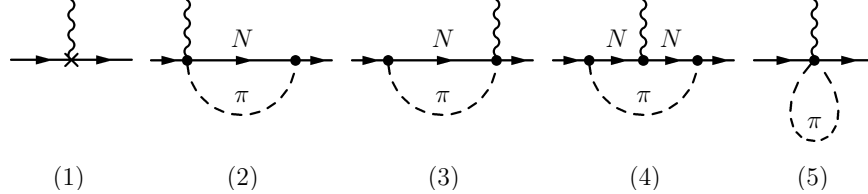


Figure 1: Diagrams contributing to the quark mass dependence of g_A up to order p^3 in Baryon Chiral Perturbation Theory. The wiggly line denotes an external isovector axial-vector field, interacting with a nucleon (solid line). The first graph to the left encodes the relevant counterterms.



Figure 2: Graph contributing to nucleon field renormalization at order p^3 .

2 g_A without explicit $\Delta(1232)$ up to $\mathcal{O}(p^4)$

The axial-vector coupling constant g_A of the nucleon is defined as the limit of the nucleon axial form factor at vanishing momentum transfer Q^2 . It is extracted from the forward (on-shell) nucleon matrix element of the isovector axial-vector quark current $\bar{q}\gamma_\mu\gamma_5(\tau^i/2)q$ where q denotes the (u, d) isospin doublet quark field and τ^i are Pauli matrices.

In this section we point out the incapability of standard chiral perturbation theory, with only pion and nucleon as explicit degrees of freedom, to deal with the quark mass dependence of g_A . The formalism has been worked out up to next-to-leading one-loop order, $\mathcal{O}(p^4)$, both in HB χ PT [15] and in the manifestly covariant framework employing infrared regularization [16]. For the sake of completeness we summarize in Appendix B technical details of the calculations with infrared regularization, from which the HB χ PT expressions can also be extracted.

The diagrams relevant at leading-one-loop level, $\mathcal{O}(p^3)$, are drawn in Figs. 1 and 2. In those loop graphs all vertices are extracted from the leading πN Lagrangian

$$\mathcal{L}_{\pi N}^{(1)} = \frac{g_A^0}{2} \bar{\Psi} \left(-\frac{1}{f_\pi} \vec{\tau} \cdot \partial_\mu \vec{\pi} + 2a_\mu \right) \gamma^\mu \gamma_5 \Psi + \dots \quad (1)$$

where Ψ is the nucleon field; g_A^0 and f_π denote, respectively, the nucleon axial coupling and the pion decay constant in the $SU(2)$ chiral limit, *i.e.* for vanishing u - and d -quark masses. Here $a_\mu = a_\mu^i \tau^i/2$ represents an external isovector axial field.

The next-to-leading-one-loop calculation involves vertices from the second order pion-nucleon Lagrangian:

$$\mathcal{L}_{\pi N}^{(2)} = 4c_1 m_\pi^2 \bar{\Psi} \Psi + \frac{c_3}{2} \text{Tr}(u_\mu u^\mu) \bar{\Psi} \Psi - \frac{c_4}{4} \bar{\Psi} \gamma^\mu \gamma^\nu [u_\mu, u_\nu] \Psi + \dots \quad (2)$$

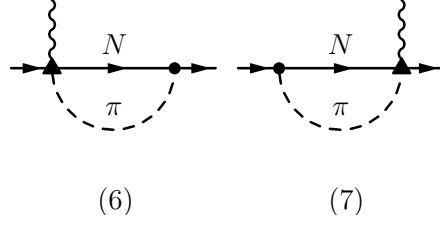


Figure 3: One-particle-irreducible fourth order diagrams contributing to g_A at the next-to-leading one-loop level. The triangle denotes a vertex appearing in $\mathcal{L}_{\pi N}^{(2)}$. The wiggly line represents an external axial vector field.

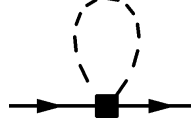


Figure 4: Graph contributing to the nucleon Z -factor at order p^4 . The square denotes a vertex from $\mathcal{L}_{\pi N}^{(2)}$ involving c_1 , c_2 and c_3 .

where

$$u_\mu = -\frac{1}{f_\pi} \vec{\tau} \cdot \partial_\mu \vec{\pi} + 2a_\mu + \dots \quad (3)$$

The trace is taken over the isospin indices. In writing down the first term of Eq. (2) we have already used the connection between pion- and u -, d -quark masses given by the Gell-Mann-Oakes-Renner relation, neglecting isospin violating effects.

The $\mathcal{O}(p^4)$ result for $g_A(m_\pi)$ is obtained by evaluating the diagrams in Fig. 3 and the contributions from wave function (Fig. 4) and mass renormalization, see Appendix B. The former ones contain the pion-nucleon-axial vertex from $\mathcal{L}_{\pi N}^{(2)}$ with the two low-energy constants c_3 and c_4 , which are known to primarily encode the influence of the Δ (1232) resonance on low-energy pion-nucleon dynamics (see for example the discussion in Ref. [17]).

The expansion of the next-to-leading one-loop expression, Eq. (45), around the chiral limit gives

$$\begin{aligned} g_A = & g_A^0 + \left[4C(\lambda) - \frac{g_A^{0\,3}}{16\pi^2 f_\pi^2} - \frac{g_A^0 + 2g_A^{0\,3}}{8\pi^2 f_\pi^2} \ln \frac{m_\pi}{\lambda} \right] m_\pi^2 + \left(\frac{g_A^0 + g_A^{0\,3}}{8\pi f_\pi^2 M_0} + \frac{2c_4 - c_3}{6\pi f_\pi^2} \right) m_\pi^3 \\ & + \left[\frac{4g_A^0(1 + 2g_A^{0\,2}) + g_A^0 M_0(3c_2 + 16c_4)}{64\pi^2 f_\pi^2 M_0^2} + 32 F(\lambda) \right. \\ & \left. + \frac{g_A^0[2 + 3g_A^{0\,2} - M_0(3c_2 + 4c_3 - 4c_4)]}{16\pi^2 f_\pi^2 M_0^2} \ln \frac{m_\pi}{\lambda} \right] m_\pi^4 + \dots \end{aligned} \quad (4)$$

Here $C(\lambda)$ and $F(\lambda)$ are effective couplings representing unresolved short-distance dynamics

and compensating logarithmic scale (λ -) dependence. The sum of the terms up to and including m_π^3 coincides with the $\mathcal{O}(p^4)$ expression in dimensionally regularized HB χ PT [15].

2.1 Numerical analysis

We analyse leading and next-to-leading one-loop expressions in comparison with an updated set of lattice QCD results for the quark mass dependence of g_A , provided by the RBCK [2], LHPC [3] and QCDSF [4] collaborations.

Fig. 5 summarizes these sets of data, although they refer to simulations with different actions, number of flavors, lattice volumes, spacings and procedures to translate the results into physical units. The reasons for the evident discrepancies between different lattice groups are not yet fully understood, see Ref. [4]. Among the data in Ref. [2] we have selected those produced on the larger lattice, with spatial size $L = 2.4$ fm. The lowest- m_π LHPC point corresponds to $L = 3.5$ fm, see [3]. Both the LHPC and QCDSF collaborations performed full-QCD simulations whereas the RBCK data are quenched. Preliminary, unquenched RBCK simulations [18] still have too large error bars to make definite statements in the region of interest.

As already mentioned, we translate the quark mass m_q -dependence of g_A into a pion mass dependence according to the Gell-Mann-Oakes-Renner relation, the leading order linear relation between m_π^2 and m_q in Chiral Perturbation Theory. Recent accurate lattice QCD results clearly display this behavior for a wide range of quark masses [19, 20, 21, 22], even for $m_\pi > 0.6$ GeV, for reasons not yet understood in detail.

In a first step the quark mass dependence of g_A in chiral perturbation theory is analysed *without fitting to the available lattice data*. We have produced Monte Carlo bands both from Eq. (34) and Eq. (45) and from the Heavy Baryon formulae at order p^3 and p^4 . In doing this we eliminate g_A^0 by imposing the physical constraint $g_A(m_\pi^{\text{phys}}) = 1.267$. The remaining parameters are randomly chosen within phenomenologically acceptable ranges. The dimension-two low-energy constants c_1, c_2, c_3 and c_4 are constrained, within non-relativistic chiral effective field theory for pions and nucleons, by several low-energy πN and NN scattering studies. Combining results of Refs. [23], [24] and [25] and simply superimposing the quoted error bars, we obtain the following ranges, in units of GeV^{-1} :

$$c_1 \approx -1.0 \dots -0.7, \quad c_2 \approx 3.1 \dots 3.5, \quad c_3 \approx -5.6 \dots -3.4, \quad c_4 \approx 3.4 \dots 3.7. \quad (5)$$

The value of c_1 basically drives the pion-nucleon sigma term. For a detailed discussion on the value of c_3 , see Ref. [17]. The analysis in Refs. [27, 28] of $\pi N \rightarrow \pi\pi N$ scattering at leading-one-loop order in HB χ PT limits the combination of couplings $C^r(\lambda)$ in Eq. (35). According to [28], $C^r(\lambda = m_\pi^{\text{phys}}) = -1.4 \pm 1.2 \text{ GeV}^{-2}$. For the higher-order couplings in the infrared regularized expressions — called F and G in Appendix B — we rely on “naive” dimensional arguments [29], at a regularization scale $\lambda = 1 \text{ GeV}$: $F^r(1 \text{ GeV}) = (-1 \dots 1) \text{ GeV}^{-4}$, $G^r(1 \text{ GeV}) = (-1 \dots 1) \text{ GeV}^{-6}$. For the nucleon mass in the chiral limit we scan the range $M_0 = (0.88 \dots 0.89) \text{ GeV}$ according to the outcome of the analysis in Refs. [17, 26].

None of the Monte Carlo bands for g_A , which include uncertainties of the low-energy parameters, comes anywhere close to the lattice data in the m_π region of interest. This is demonstrated in Fig. 5 for the case of the $\mathcal{O}(p^4)$ Heavy Baryon expression. What numerically drives the trend of the quark mass dependence of g_A at order p^4 is the combination of c_3 and c_4 in the term proportional to m_π^3 in Eq. (4)¹. Recoil corrections to the non-relativistic results which one gets in the infrared regularization approach, do not improve the situation.

We can conclude at this point that chiral perturbation theory of the pion-nucleon system, at order p^4 and without explicitly propagating $\Delta(1232)$, fails in the attempt to provide an interpolation of g_A between the physical point and lattice QCD results. The price one would have to pay for enforcing adjustment of an interpolating curve to the lattice data is that the combination $2c_4 - c_3$ of πN low-energy constants must be tuned to a value totally inconsistent with the empirical ones. For chiral perturbation theory to be able to make contact with present lattice data, compensation of the strong m_π^3 trend must come from higher powers of m_π . In a recent paper [7] a relatively flat quark mass dependence is shown to be possibly achieved at two-loop level in the Heavy Baryon framework. In this approach the compensation of the m_π^3 term does not arise from the “double log” piece characteristic of the two-loop calculation but from a fine-tuning of unknown effective couplings at fifth order. The theoretical uncertainties are reported to be acceptably small only for $m_\pi \lesssim 300$ MeV.

A more efficient and physically motivated way to successfully interpolate between lattice results and the physical point is to include explicit $\Delta(1232)$ degrees of freedom [6]. This leads to a whole string of higher powers in m_π already at leading-one-loop level and the outcome of the fits agrees favourably with available information from low-energy hadron phenomenology, see Section 4.1. Intermediate $\Delta(1232)$ contributions are well-known to play a crucial role in axial current matrix elements because the axial-vector field induces strong isovector $N(1/2^+) \rightarrow \Delta(3/2^+)$ transitions [30]. The near degeneracy of the $\Delta(1232)$ with the nucleon suggests treating both N and Δ as explicit degrees of freedom. Before focusing on the detailed formalism in Section 4, it is useful to recall, in the next section, some well-known basic physics which outlines the special relevance of the $\Delta(1232)$ in the present context of g_A .

3 Adler-Weisberger sum rule and a schematic model

The Adler-Weisberger (AW) sum rule [31] combines information from low-energy QCD, current algebra and dispersion relations to connect low-energy parameters of the πN system (f_π and g_A) with an integral over the difference of the $\pi^+ p$ and $\pi^- p$ total cross-sections. Using the Goldberger-Treiman relation and the Weinberg-Tomozawa low-energy theorem [32] one obtains²

$$g_A^2 = 1 + \frac{2f_\pi^2}{\pi} \int_0^\infty \frac{dq}{\omega} [\sigma_{\pi^+ p}(\omega) - \sigma_{\pi^- p}(\omega)] + \mathcal{O}\left(\frac{m_\pi^2}{M_N^2}\right), \quad (6)$$

¹The large contribution associated with the m_π^3 term was already pointed out in Ref. [15].

²See, for example, the derivation in [30].

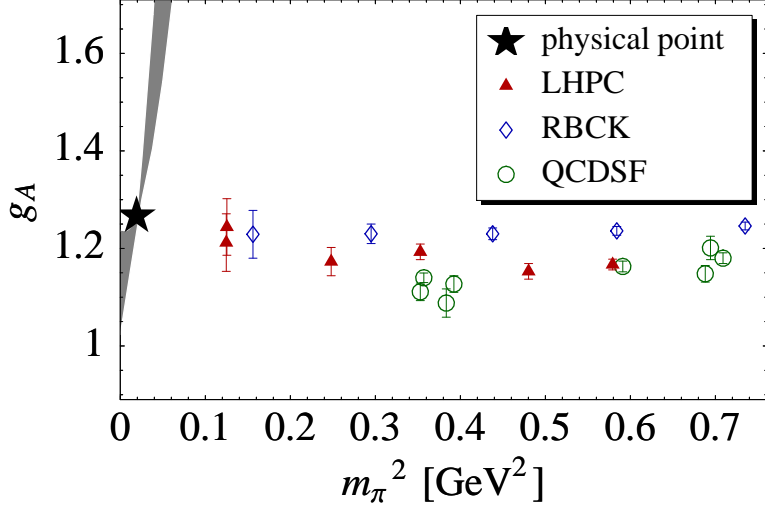


Figure 5: Data base of lattice QCD results for the pion mass dependence of g_A provided by the RBCK [2], QCDSF [4] and LHPC [3] collaborations. Also shown is the $\mathcal{O}(p^4)$ result for $g_A(m_\pi)$ in Heavy Baryon χ PT, with the physical point included as a constraint. The band reflects the uncertainty on the input values of the low-energy constants involved.

where the integral is taken over the pion momentum, $q = |\vec{q}| = \sqrt{\omega^2 - m_\pi^2}$, and ω denotes the pion energy in the nucleon rest frame. The deviation of g_A from 1 is tied to pion-nucleon dynamics and spontaneous (and explicit) chiral symmetry breaking. The left- and right-hand sides of the sum rule turn out to agree at the percent level using $f_\pi = 92.4$ MeV and an accurate parameterization of the measured $\pi^\pm p$ cross-sections [33].

In order to demonstrate the prominent role of the $\Delta(1232)$ in the AW sum rule for g_A it is instructive to perform a simple schematic model calculation as follows. Consider the P -wave πN forward scattering amplitudes $f_\alpha(\omega)$ in spin-isospin channels $\alpha = (2I, 2J)$. Their contributions to the total πN cross section is

$$\sigma_\alpha(\omega) = \frac{4\pi}{|\vec{q}|} \text{Im} f_\alpha(\omega) \quad (7)$$

according to the optical theorem. Next, introduce the K -matrix K_α in each channel by

$$f_\alpha(\omega) = \frac{K_\alpha(\omega)}{1 - i |\vec{q}| K_\alpha(\omega)} . \quad (8)$$

K_α has poles on the real ω -axis located at the physical masses of the corresponding N and Δ intermediate states.

Starting from the πNN vertex Eq. (1) and the leading-order $\pi N\Delta$ transition Lagrangian

$$\mathcal{L}_{\pi N\Delta}^{(1)} = -\frac{c_A}{f_\pi} \bar{\Psi}_\mu^i \partial^\mu \pi^i \Psi + \text{h. c.} , \quad (9)$$

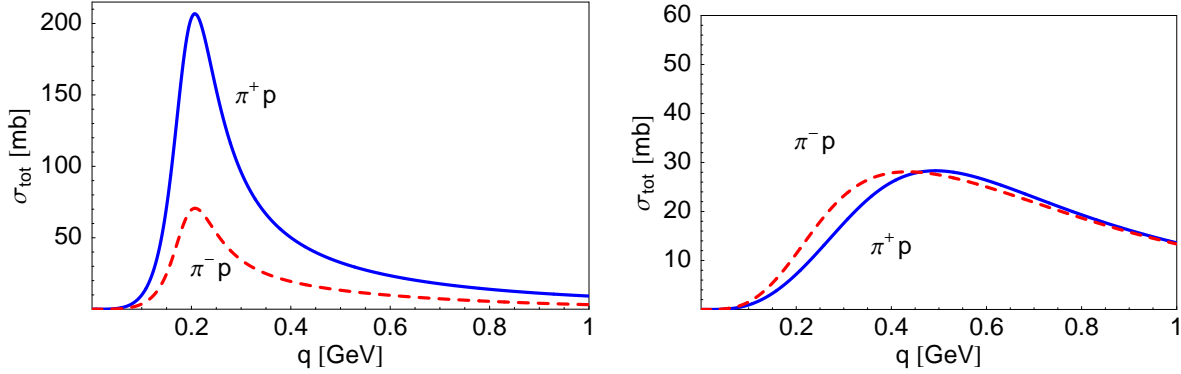


Figure 6: P -wave contributions from the nucleon and Δ (1232) pole graphs to the total $\pi^+ p$ and $\pi^- p$ cross sections, plotted against the pion momentum in the laboratory frame. In the left panel the direct and crossed Δ (1232)-pole graphs are included, in the right panel not.

where Ψ_μ^i is the Rarita-Schwinger field of the Δ , the K -matrix pieces involving direct and crossed N and Δ pole terms are, in the non-relativistic limit [34]:

$$\begin{aligned} K_{33} &= \frac{\vec{q}^2}{12\pi f_\pi^2} \left[\frac{g_A^2}{\omega} + \frac{c_A^2}{\Delta - \omega} + \frac{1}{9} \frac{c_A^2}{\Delta + \omega} \right] , \\ K_{11} &= \frac{\vec{q}^2}{3\pi f_\pi^2} \left[-\frac{g_A^2}{2\omega} + \frac{4}{9} \frac{c_A^2}{\Delta + \omega} \right] , \\ K_{13} &= K_{31} = \frac{1}{4} K_{11} , \end{aligned} \quad (10)$$

where $\Delta = M_\Delta - M_N$ is the delta-nucleon mass splitting deduced from the position of the resonance pole in the complex center-of-mass energy plane.

We use $f_\pi = 92.4$ MeV on the right-hand sides of these last equations, together with $\Delta = 271.1$ MeV, the delta pole position determined empirically from magnetic dipole and electric quadrupole transition amplitudes [35], and $c_A = 1.5$ from the $\Delta \rightarrow \pi N$ decay width (see for example Ref. [17]). Then the P -wave πN scattering volumes deduced from Eq. (10) at $\omega = m_\pi$ agree very well with experiment, see also Ref. [34]. Eq. (8) and the optical theorem lead to the P -wave contributions to the total $\pi^+ p$ and $\pi^- p$ cross-sections:

$$\sigma_{\pi^+ p} = \frac{4\pi}{|\vec{q}|} \text{Im} [2f_{33} + f_{31}] , \quad \sigma_{\pi^- p} = \frac{4\pi}{3|\vec{q}|} \text{Im} [2f_{33} + f_{31} + 4f_{13} + 2f_{11}] . \quad (11)$$

They are drawn in the left panel of Fig. 6. The curves are in good agreement with the empirical ones from near threshold up to $q \approx 0.5$ GeV [33, 34], while the region between 0.5 and 2 GeV receives contributions from higher resonances. Using the cross-sections in Eq. (6), we obtain $g_A = 1.22$. The integral on the right-hand side of the Adler-Weisberger sum rule is indeed dominated by the contribution of the Δ (1232) to the πN scattering amplitude. If the calculation includes only the nucleon Born terms from Eqs. (10), setting $c_A = 0$, $\sigma_{\pi^\pm p}$ change as shown in the right panel of Fig. 6. “Switching off” the $\pi N \Delta$ coupling,

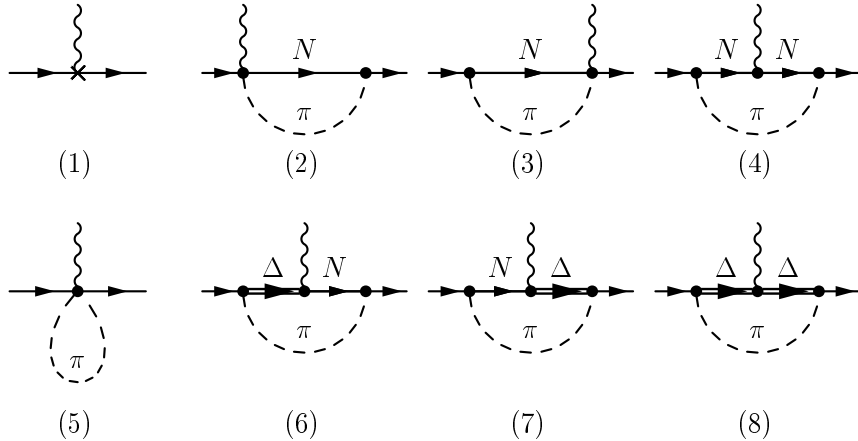


Figure 7: g_A in the Small Scale Expansion at leading-one-loop order. The wiggly line denotes an external isovector axial-vector field. All vertices shown here appear in the leading πN and $\pi N \Delta$ Lagrangians.

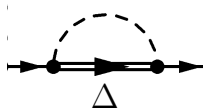


Figure 8: Graph contributing to wave function renormalization at order ϵ^3 .

the contribution from the dispersion integral in the Adler-Weisberger sum rule changes sign and g_A is reduced to 0.99.

This non-relativistic, tree-level calculation illustrates the role of the $\Delta(1232)$ at the physical pion mass. In our previous paper [6] we have also shown that treating the $\Delta(1232)$ as an explicit degree of freedom leads to successful chiral extrapolation for pion masses well above m_π^{phys} . The lattice results used there are now outdated by more recent and improved sets. In the next section we check whether our conclusions in Ref. [6] remain unaltered for the most recent input data and perform a detailed statistical analysis, using the same methods as described in Ref. [17].

4 g_A with explicit $\Delta(1232)$

In the framework of the so-called Small Scale Expansion (SSE) [36], the delta-nucleon mass splitting Δ is treated as a small parameter and included in the power counting of “small scales” generically denoted by ϵ . The leading one-loop, order ϵ^3 , contribution to g_A is represented by the diagrams in Figs.7 and 8. We recall here the result in the continuum

and infinite volume case with dimensional regularization [6]:

$$\begin{aligned}
g_A^{\text{SSE}}(m_\pi^2) = & g_A^0 - \frac{g_A^{0\,3} m_\pi^2}{16\pi^2 f_\pi^2} + 4 \left[C^{\text{SSE}}(\lambda) + \frac{c_A^2}{4\pi^2 f_\pi^2} \left(\frac{155}{972} g_1 - \frac{17}{36} g_A^0 \right) + \gamma^{\text{SSE}} \ln \frac{m_\pi}{\lambda} \right] m_\pi^2 \\
& + \frac{4c_A^2 g_A^0}{27\pi f_\pi^2 \Delta} m_\pi^3 + \frac{8}{27\pi^2 f_\pi^2} c_A^2 g_A^0 m_\pi^2 \sqrt{1 - \frac{m_\pi^2}{\Delta^2}} \ln R \\
& + \frac{c_A^2 \Delta^2}{81\pi^2 f_\pi^2} (25g_1 - 57g_A^0) \left(\ln \frac{2\Delta}{m_\pi} - \sqrt{1 - \frac{m_\pi^2}{\Delta^2}} \ln R \right) + \mathcal{O}(\epsilon^4) , \quad (12)
\end{aligned}$$

with

$$\begin{aligned}
\gamma^{\text{SSE}} = & \frac{-1}{16\pi^2 f_\pi^2} \left[g_A^0 \left(\frac{1}{2} + g_A^{0\,2} \right) + \frac{2}{9} c_A^2 \left(g_A^0 - \frac{25}{9} g_1 \right) \right] , \\
R = & \frac{\Delta}{m_\pi} + \sqrt{\frac{\Delta^2}{m_\pi^2} - 1} .
\end{aligned} \quad (13)$$

$C^{\text{SSE}}(\lambda)$ is a combination of renormalized third-order couplings, cf. Eq. (35), and g_1 is the axial delta-delta coupling; f_π and Δ are the $SU(2)$ chiral limit values of the pion decay constant and the delta nucleon mass splitting, respectively. See Ref. [6] for further details. The analytic continuation of the previous expression for $m_\pi > \Delta$ is achieved via the replacement

$$\sqrt{\Delta^2 - m_\pi^2} \ln \left(\sqrt{\frac{\Delta^2}{m_\pi^2} - 1} + \frac{\Delta}{m_\pi} \right) \rightarrow -\sqrt{m_\pi^2 - \Delta^2} \arccos \left(\frac{\Delta}{m_\pi} \right) . \quad (14)$$

Note that in Eq. (12) decoupling of the delta has been implemented up to working order [4, 6]. As a result, g_A^0 is the same coupling as in HB χ PT calculations without explicit delta. This is different in Ref. [9].

4.1 Fit results

We have performed fits based on Eq. (12) and its analytic continuation for $m_\pi > \Delta$ both to the two-flavor, quenched RBCK data and the full-QCD, 2 (lighter) + 1 (heavier)-flavor LHPC results. From the RBCK data we have selected the three points with the lightest pion masses. The values of f_π , c_A and Δ have been fixed as input. Without any loss of generality we have set the regularization scale λ equal to 1 GeV. The effective coupling $C^{\text{SSE}}(\lambda = 1 \text{ GeV})$ has been eliminated by imposing that the fit curves pass through the physical point.

Fig. 9 and Table 1 summarize our results for the LHPC data. In drawing the $1-\sigma$ error band (which takes into account correlations between the parameters), we set f_π equal to its physical value and $c_A = 1.5$. Furthermore, $\Delta = 271.1$ MeV from the real part of the complex delta pole in the total center-of-mass energy plane [35].

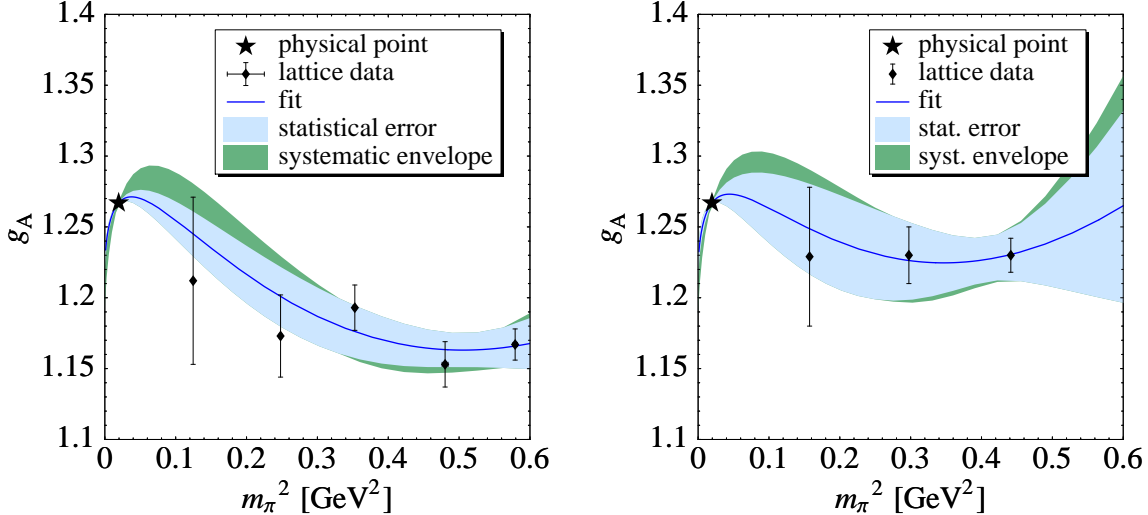


Figure 9: $\mathcal{O}(\epsilon^3)$ SSE best-fit curves, 68%-statistical error bands and systematic envelopes for the LHPC lattice results [3] (left) and RBCK data [2] (right). The physical point is included as a constraint. See Table 1.

The “systematic band” [17] in Fig. 9 quantifies the sensitivity to variations of the input parameters. It is given by the envelope of the $1-\sigma$ bands scanning also the additional input values $f_\pi = 86.2$ MeV [37], $c_A = 1.125$ [6] and $\Delta = 293$ MeV (from the 90^0 πN phase-shift in the spin-3/2 isospin-3/2 channel [1]). We point out that the constant g_1 appears only in combinations multiplied by c_A^2 . This is evident from diagram (8) of Fig. 7. In the fit using $c_A = 1.125$, the apparent strong deviation of g_1 from the $SU(4)$ quark model prediction $g_1 = 9g_A/5 \approx 2.2$ is therefore of little relevance. The range accessible to $c_A^2 g_1$ is indeed much smaller than that for g_1 itself, see Table 1.

Our estimate of $C^{\text{SSE}}(1 \text{ GeV})$ is consistent with (limited) information from $\pi N \rightarrow \pi\pi N$ scattering. One can indeed link $C^{\text{HB}}(\lambda)$ in the Heavy Baryon πN effective field theory and $C^{\text{SSE}}(\lambda)$ in the framework with explicit delta. Comparing the terms proportional to m_π^2 in the chiral expansion of Eq. (12) and Eq. (39), one gets:

$$C^{\text{HB}}(\lambda) = C^{\text{SSE}}(\lambda) + \frac{c_A^2}{72\pi^2 f_\pi^2} \left[5 \left(\frac{23}{27} g_1 - \frac{7}{3} g_A^0 \right) + \left(\frac{25}{9} g_1 - g_A^0 \right) \ln \frac{2\Delta}{\lambda} \right]. \quad (15)$$

According to our fits we obtain $C^{\text{HB}}(\lambda = m_\pi^{\text{phys}}) = (-0.45 \pm 0.05) \text{ GeV}^{-2}$, consistent with the broad range of values extracted from Ref. [28]. In agreement with [6], we stress that the “chiral log” in the leading non-analytic quark-mass term is only visible for pion masses *well below* the physical point.

We have also performed fits to the three LHPC points below 600 MeV in pion mass only. The outcome is compatible, within large error bars, with our previous results for $m_\pi \lesssim 760$ MeV in Table 1.

Table 1: Fit results for the $\mathcal{O}(\epsilon^3)$ SSE interpolation between the physical value of g_A and the LHP points [3].

	(a) statistical error	(b) systematic envelope
g_A^0	1.224 ± 0.004 fitted	$1.191 \dots 1.228$ fitted
g_1	2.80 ± 0.12 fitted	$2.6 \dots 6.0$ fitted
$C^{\text{SSE}}(1 \text{ GeV}) \text{ (GeV}^{-2})$	-1.65 ± 0.17 elim.	$-4.3 \dots -1.4$ elim.
f_π (MeV)	92.4 fixed	86.2 ... 92.4 scanned
c_A	1.5 fixed	1.12 ... 1.5 scanned
Δ (MeV)	271.1 fixed	271 ... 293 scanned
$\chi^2/\text{d.o.f.}$	0.93	0.92 ... 1.27
$c_A^2 g_1$	6.29 ± 0.27	$5.9 \dots 7.6$
$C^{\text{HB}}(m_\pi^{\text{phys}}) \text{ (GeV}^{-2})$	-0.45 ± 0.05	$-0.55 \dots 0.41$

Table 2 summarizes our study of the RBCK data. The error bars of the output parameters absorb the effects of one heavier flavor, together with the above mentioned systematic discrepancies due to different fermion actions, (un)quenching, and translation of lattice results into physical units.

4.2 Expanding in powers of m_π

The effective field theory framework with explicit $\Delta(1232)$ degrees of freedom offers a way of studying convergence properties of πN chiral perturbation theory. We perform such a test using the $\mathcal{O}(\epsilon^3)$ non-relativistic SSE expression which is able to describe the quark mass dependence of g_A over a large range of pion masses. We expand the expression (12) for $m_\pi < \Delta$ in powers of m_π , around the chiral limit. The resulting series is of the form:

$$\begin{aligned}
g_A &= g_A^0 \left\{ 1 + \left[\alpha_2 \ln \frac{m_\pi}{\lambda} + \tilde{\alpha}_2 \ln \frac{2\Delta}{\lambda} + \beta_2 \right] m_\pi^2 + \alpha_3 \frac{m_\pi^3}{\Delta} \right. \\
&\quad \left. + \sum_{n \geq 2} \gamma_n \frac{m_\pi^{2n}}{\Delta^{2n-2}} \ln \frac{m_\pi}{2\Delta} + \sum_{n \geq 2} \beta_n \frac{m_\pi^{2n}}{\Delta^{2n-2}} \right\} + \mathcal{O}(\epsilon^4) \\
&= g_A^0 \left[1 + A m_\pi^2 \ln \frac{m_\pi}{\lambda} + B(\lambda) m_\pi^2 + C m_\pi^3 + D m_\pi^4 \ln \frac{m_\pi}{\lambda} + E(\lambda) m_\pi^4 + \dots \right] \quad (16)
\end{aligned}$$

All terms can be mapped onto the πN Heavy Baryon expansion, according to the decoupling theorem [38, 39]. The series in m_π^n/Δ^m in the last equation corresponds to “integrating out” explicit delta degrees of freedom. The intermediate delta contributions are embedded in a string of couplings appearing in the Heavy Baryon Lagrangian. We note that in Eq. (16) the terms starting from m_π^3 come entirely from diagrams 6 - 8 in Fig. 7. For $m_\pi < \Delta$ a detailed numerical analysis of Eq. (16) therefore gives an impression of the systematic errors introduced by integrating out the leading-order effect of the $\Delta(1232)$ in the HB χ PT expansion.

Table 2: Fit results for the $\mathcal{O}(\epsilon^3)$ SSE interpolation between the physical value of g_A and the three RBCK points lightest in pion mass with $L = 2.4$ fm [2].

	(a) statistical error	(b) systematic envelope
g_A^0	1.223 ± 0.007 fitted	$1.189 \dots 1.230$ fitted
g_1	2.83 ± 0.26 fitted	$2.5 \dots 6.5$ fitted
$C^{\text{SSE}}(1 \text{ GeV}) \quad (\text{GeV}^{-2})$	-1.67 ± 0.37 elim.	$-4.7 \dots -1.3$ elim.
$f_\pi \quad (\text{MeV})$	92.4 fixed	$86.2 \dots 92.4$ scanned
c_A	1.5 fixed	$1.12 \dots 1.5$ scanned
$\Delta \quad (\text{MeV})$	271.1 fixed	$271 \dots 293$ scanned
$\chi^2/\text{d.o.f.}$	0.2	$0.19 \dots 0.46$
$c_A^2 g_1$	6.4 ± 0.6	$5.7 \dots 8.2$
$C^{\text{HB}}(m_\pi^{\text{phys}}) \quad (\text{GeV}^{-2})$	-0.43 ± 0.11	$-0.6 \dots 0.5$

Fig. 10 shows the convergence properties of the series (16) towards the full $\mathcal{O}(\epsilon^3)$ result in Eq. (12). In Fig. 11 we plot the difference δg_A between the expansion truncated at some power of m_π and the full expression, for fixed values of the pion mass. In those plots we set g_A^0 , C^{SSE} and g_1 equal to their central values in the fit to the LHPD data, see Table 1.

For small values of m_π the expansion exhibits fast convergence. As soon as m_π becomes larger than Δ we are outside the radius of convergence of the series in Eq. (16). However, up to about 300 MeV in pion mass, the expansion truncated for example at m_π^4 still yields a good approximation. This is consistent with Ref. [7] where a fifth-order counterterm proportional to m_π^4 turns out to be necessary and sufficient in the Heavy Baryon framework to get in contact with the smallest- m_π lattice data.

For $m_\pi > \Delta$ the expansion (16) behaves like an asymptotic series [40]. For a given value of m_π there is an optimal truncation order giving minimal deviation from the full result. Beyond this order any truncation worsens the result. We find also that the optimal order shifts to lower powers when increasing the pion mass. At some value of m_π the deviation, even at the best truncation order, exceeds the required level of precision.

Our analysis suggests that for $m_\pi \gtrsim 300$ MeV, once the pion mass exceeds the ΔN mass difference, the systematic errors in the Heavy Baryon expansion induced by removing the $\Delta(1232)$ as an explicit degree of freedom tend to get out of control. The series in Eq. (16) is of course only part of the full Heavy Baryon result. It is thus in principle possible that the observed deviation δg_A can be compensated by other higher order terms in the diagrammatic expansion.

At this point it is worth noting that a reliable expression for the quark mass dependence of g_A is crucial in order to consistently describe the quark mass dependence of the nucleon mass in the Heavy Baryon scheme at order p^5 [41, 42]. Our numerical analysis suggests that this cannot be achieved for $m_\pi \gtrsim 300$ MeV in a chiral effective field theory scheme restricted to pion and nucleon degrees of freedom only.

We have explored the sensitivity of our convergence study to g_1 , which controls the

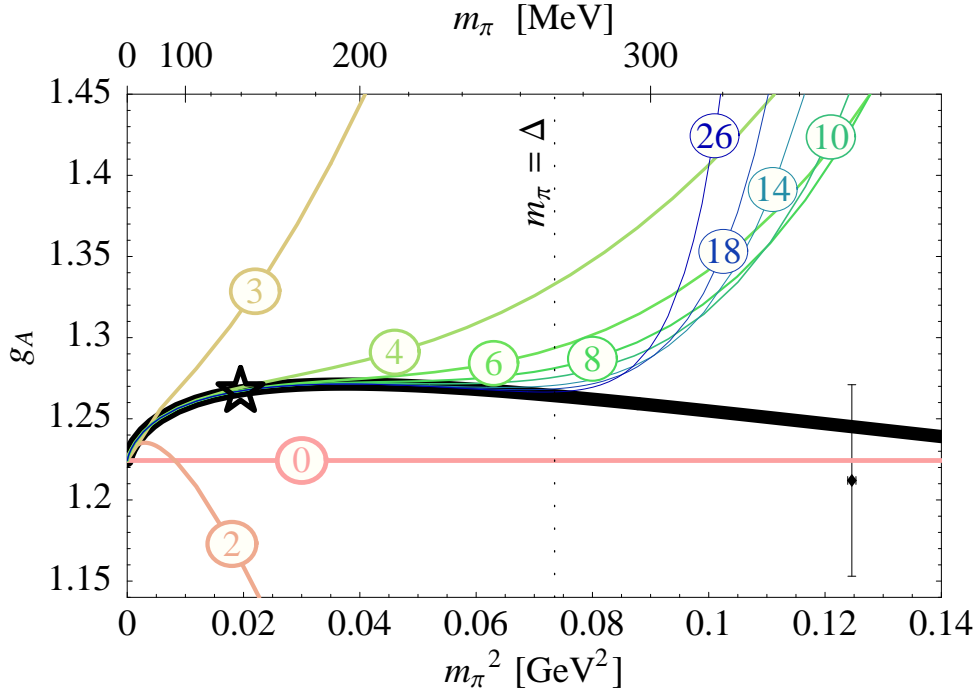


Figure 10: g_A in SSE at order ϵ^3 : expansion in powers of m_π . Parameters have been set equal to the central values in the fit to the LHPC data. The labels n of the curves give the order m_π^n at which the series is truncated. The star denotes the physical point. The LHPC data point with smallest m_π is also displayed.

relative strength of competing structures in the $\mathcal{O}(\epsilon^3)$ SSE formula (12). We observed that for the rather ‘‘large’’ value $g_1 \approx 6$ an m_π^4 -approximation is quite close to the SSE result for a large range of pion masses. We interpret this as a warning that an effective theory can spuriously appear to be well behaved at a specific truncation order for a particular artificial choice of parameters. This is in agreement with Ref. [7] where the two-loop Heavy Baryon expression is found to describe the trend shown by lattice data up to $m_\pi \approx 600$ MeV just for a particular choice of effective low-energy couplings.

Our analysis is based on the validity of the SSE perturbative framework. Our fits support the conclusion that in SSE important quark-mass dependent effects for g_A , involving the $\Delta(1232)$, are moved to low perturbative orders in the diagrammatic expansion. However, before any firm conclusion can be drawn it is mandatory to study the effects of higher-order corrections and check the stability of our results. It is needless to say that for a numerical study at $\mathcal{O}(\epsilon^4)$, we must either wait for an improvement of the statistics for the g_A lattice data or perform a combined analysis of g_A and other nucleon observables characterized by a common subset of low-energy constants.

5 Conclusions

Summarizing the main results of this (continuum and infinite volume) analysis of g_A , we conclude as follows:

- Heavy Baryon Chiral Perturbation Theory restricted to pion and nucleon degrees of freedom only, when applied up to and including next-to-next-to-leading order, fails in attempts to produce meaningful interpolations between g_A at the physical point and present lattice data.
- The explicit inclusion of the $\Delta(1232)$ at leading one-loop level, as implemented for example in the Small Scale Expansion scheme, is crucial in order to get a satisfactory description of the quark mass dependence of g_A from the chiral limit across the physical point up to the lattice data. This does not come as a surprise in view of the well-known Δ -dominance of πN interactions and the Adler-Weisberger sum rule.
- An expansion of the leading one-loop expression with explicit $\Delta(1232)$ in powers of m_π exhibits a stable convergence pattern only for pion masses below 300 MeV, the characteristic scale of the delta-nucleon mass difference. For larger values of m_π the expansion behaves like an asymptotic series. Not unexpectedly, our analysis suggests that the systematic errors induced in the Heavy Baryon expansion by integrating out the $\Delta(1232)$, get out of control for $m_\pi \gtrsim 300$ MeV.
- The addition of one heavier flavor in lattice simulations yields interpolation results that are statistically compatible with the two-flavor case.

6 Acknowledgments

We thank U.-G. Meißner, K. Orginos, D. B. Renner, D. Richards for helpful discussions. B. M. acknowledges support by the DFG Emmy Noether-program. This work has been supported in part by BMBF and DFG.

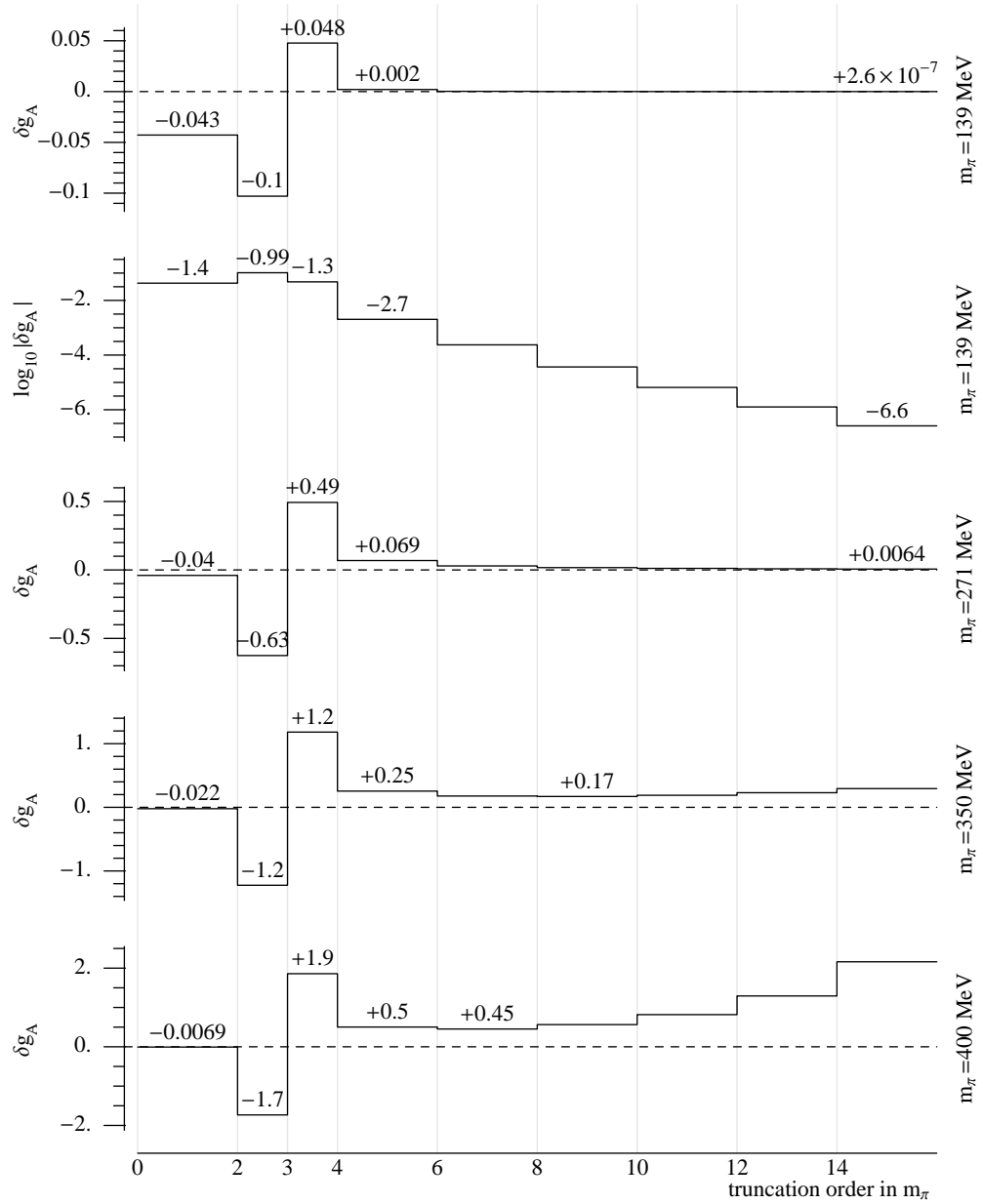


Figure 11: g_A in SSE: convergence plot for the expansion of the $\mathcal{O}(\epsilon^3)$ result in powers of m_π . The dotted line refers to the full result with parameters set equal to the central values in the fit to the LHC data.

Appendix

A d -dimensional one-loop integrals

We encounter pion loop integrals in $d = 4$ dimensions of the following basic type:

$$\Delta_\pi(m_\pi^2) = \frac{1}{i} \int \frac{d^d k}{(2\pi)^d} \frac{1}{m_\pi^2 - k^2 - i\epsilon} = m_\pi^{d-2} (4\pi)^{-d/2} \Gamma\left(1 - \frac{d}{2}\right) . \quad (17)$$

Any ultraviolet divergence as d tends to 4 is subsumed in

$$L(\lambda) = \frac{\lambda^{d-4}}{16\pi^2} \left\{ \frac{1}{d-4} - \frac{1}{2} \left[\ln(4\pi) + \Gamma'(1) + 1 \right] \right\} , \quad (18)$$

where λ is the dimensional regularization scale. Consequently,

$$\Delta_\pi(m_\pi^2) = 2m_\pi^2 \left[L(\lambda) + \frac{1}{16\pi^2} \ln \frac{m_\pi}{\lambda} \right] . \quad (19)$$

For loop integrals involving a nucleon propagator, consider the infrared singular part, cf. [11], denoted by a subscript I attached to the integral:

$$I_N(p^2, m_\pi^2) = \frac{1}{i} \int_I \frac{d^d k}{(2\pi)^d} \frac{1}{(m_\pi^2 - k^2 - i\epsilon)[M_0^2 - (p-k)^2 - i\epsilon]} \quad (20)$$

$$= -\frac{p^2 - M_0^2 + m_\pi^2}{p^2} L(\lambda) + \bar{I}_N(p^2, m_\pi) , \quad (21)$$

$$\begin{aligned} \bar{I}_N(p^2, m_\pi^2) &= -\frac{1}{8\pi^2} \frac{\alpha\sqrt{1-\Omega^2}}{1+2\alpha\Omega+\alpha^2} \arccos\left(-\frac{\Omega+\alpha}{\sqrt{1+2\alpha\Omega+\alpha^2}}\right) \\ &\quad - \frac{1}{16\pi^2} \frac{\alpha(\alpha+\Omega)}{1+2\alpha\Omega+\alpha^2} \left(2 \ln \frac{m_\pi}{\lambda} - 1\right) \end{aligned} \quad (22)$$

$$\text{with } \alpha = \frac{m_\pi}{M_0}, \quad \Omega = \frac{p^2 - m_\pi^2 - M_0^2}{2m_\pi M_0} . \quad (23)$$

Furthermore,

$$p^\mu I_N^{(1)}(p^2, m_\pi^2) = \frac{1}{i} \int_I \frac{d^d k}{(2\pi)^d} \frac{k^\mu}{(m_\pi^2 - k^2 - i\epsilon)[M_0^2 - (p-k)^2 - i\epsilon]} . \quad (24)$$

Using

$$p \cdot k = \frac{1}{2}(p^2 - M_0^2 + m_\pi^2) + \frac{1}{2}(k^2 - m_\pi^2) - \frac{1}{2}[(p - k)^2 - M_0^2] , \quad (25)$$

one finds

$$I_N^{(1)}(p^2, m_\pi^2) = \frac{1}{2p^2} [(p^2 - M_0^2 + m_\pi^2) I_N(p^2, m_\pi^2) + \Delta_\pi(m_\pi^2)] . \quad (26)$$

We use the following notations:

$$I_N \equiv I_N(p^2 = M_0^2, m_\pi^2), \quad I_N^{(1)} \equiv I_N^{(1)}(p^2 = M_0^2, m_\pi^2), \quad (27)$$

$$I_\Delta(p^2) \equiv I_N(p^2, M_0 \rightarrow M_\Delta^0), \quad I_\Delta \equiv I_\Delta(p^2 = M_0^2, m_\pi^2) . \quad (28)$$

B Details on the $\mathcal{O}(p^3)$ and $\mathcal{O}(p^4)$ calculations

At order p^3 , nucleon field renormalization contributes in the way shown in Fig. 2. At this level of accuracy, the nucleon self-energy $\Sigma(p)$ is approximated as

$$\Sigma(\not{p} = M_N) \approx \Sigma(\not{p} = M_0) , \quad (29)$$

where M_0 is the nucleon mass in the $SU(2)$ chiral limit. This implies for the nucleon wave-function renormalization factor:

$$Z_N \approx 1 + \left. \frac{\partial \Sigma^{(3)}}{\partial \not{p}} \right|_{\not{p}=M_0} . \quad (30)$$

Here $\Sigma^{(3)}$ is the nucleon self-energy at order p^3 . Using infrared regularization [11],

$$\Sigma^{(3)} = \frac{3g_A^0}{4f_\pi^0} (M_0 + \not{p}) \left[m_\pi^2 I_N(p^2, m_\pi^2) + (M_0 - \not{p}) \not{p} I_N^{(1)}(p^2, m_\pi^2) \right] \quad (31)$$

in terms of the basic integrals in Appendix A. Hence one finds:

$$\begin{aligned} Z_N = 1 & - \frac{1}{32\pi^2 f_\pi^2 M_0^3 \sqrt{4 - m_\pi^2/M_0^2}} \left\{ 3g_A^{0\,2} m_\pi^2 \left[(2m_\pi^3 - 6M_0^2 m_\pi) \arccos\left(-\frac{m_\pi}{2M_0}\right) \right. \right. \\ & + M_0 \sqrt{4 - \frac{m_\pi^2}{M_0^2}} \left(M_0^2 (1 + 48\pi^2 L(\lambda)) - 32\pi^2 L(\lambda) m_\pi^2 + (3M_0^2 - 2m_\pi^2) \ln \frac{m_\pi}{\lambda} \right) \left. \right] \left\} \right. \\ & - 8B_{20} m_\pi^2 + 32 F_2 m_\pi^4 , \end{aligned} \quad (32)$$

where $L(\lambda)$ is defined in Eq. (18). Here B_{20} is a third-order coupling [6], while F_2 enters in a fifth-order counterterm required to absorb the divergence proportional to m_π^4 .

Projecting out the contributions to g_A from the leading-one-loop amplitudes in Fig. 1, the following expression results, given in terms of the integrals in Appendix A:

$$\begin{aligned} g_A = g_A^0 Z_N & + 4 B_9 m_\pi^2 - \frac{g_A^0}{f_\pi^2} \Delta_\pi - 2 \frac{g_A^0}{f_\pi^2} m_\pi^2 I_N + \frac{g_A^{0\,3}}{4(d-1)f_\pi^2 M_0} \left[2m_\pi^2 M_0 (d-3) I_N \right. \\ & \left. + (2(d-3)M_0^2 m_\pi^2 + m_\pi^4) \left. \frac{\partial}{\partial M_0} I_N(p^2) \right|_{p^2=M_0} + (d-3) M_0 \Delta_\pi \right] + 32 F_1 m_\pi^4 . \end{aligned} \quad (33)$$

B_9 is the third-order coupling already introduced in Ref. [6] and F_1 takes care of an ultraviolet divergence.

Combining Eq. (32) and Eq. (33), the result for the pion mass dependence of g_A at order

p^3 with infrared regularization is given by

$$\begin{aligned}
g_A = & \frac{1}{16\pi^2 f_\pi^2 M_0^3 \sqrt{4 - m_\pi^2/M_0^2}} \left\{ g_A^0 m_\pi^3 (8(g_A^{0^2} + 1)M_0^2 - (3g_A^{0^2} + 2)m_\pi^2) \arccos\left(-\frac{m_\pi}{2M_0}\right) \right. \\
& - M_0 \sqrt{4 - \frac{m_\pi^2}{M_0^2}} \left[M_0^2 m_\pi^2 g_A^{0^3} + (m_\pi^4 - 16f_\pi^2 M_0^2 \pi^2) g_A^0 \right. \\
& \left. \left. + ((4g_A^{0^2} + 2)g_A^0 m_\pi^2 M_0^2 - (3g_A^{0^2} + 2)g_A^0 m_\pi^4) \ln \frac{m_\pi}{\lambda} - 64C^r(\lambda) f_\pi^2 M_0^2 m_\pi^2 \pi^2 \right] \right\} \\
& + 32F^r(\lambda) m_\pi^4. \tag{34}
\end{aligned}$$

For the couplings involved in third order counterterms we use the notation already employed in our previous paper [6]:

$$C^r(\lambda) \equiv B_9^r(\lambda) - 2g_A^0 B_{20}^r(\lambda). \tag{35}$$

Furthermore, $F^r(\lambda) = F_1^r(\lambda) + F_2^r(\lambda)$. Those effective couplings are renormalized and regularization-scale- λ -dependent. They encode short-distance dynamics effects and scale in just such a way that the right-hand side of Eq. (34) is scale independent:

$$C^r(\lambda) = B_9 - 2g_A^0 B_{20} - \frac{L(\lambda)}{f_\pi^2} \left(\frac{1}{2} g_A^0 + g_A^{0^3} \right) \tag{36}$$

$$F^r(\lambda) = F + \frac{L(\lambda)}{32f_\pi^2 M_0^2} g_A^0 (2 + 3g_A^{0^2}). \tag{37}$$

The factor 32 in the fifth-order counterterm in Eq.(34) emphasizes that F is the effective coupling to which one should apply “naive” dimensional arguments, cf. Ref. [29]. Indeed the effective πN Lagrangian at order p^5 can contribute via

$$\mathcal{L}_{\pi N}^{(5)} = 32 f m_\pi^4 \bar{\Psi} a_\mu \gamma^\mu \gamma_5 \Psi + \dots \tag{38}$$

where we expect $f = \mathcal{O}(1/\Lambda_\chi^4)$.

Expanding Eq.(34) around $m_\pi = 0$ leads to

$$\begin{aligned}
g_A = & g_A^0 + \left[4C^r(\lambda) - \frac{g_A^{0^3}}{16\pi^2 f_\pi^2} - \frac{g_A^0 + 2g_A^{0^3}}{8\pi^2 f_\pi^2} \ln \frac{m_\pi}{\lambda} \right] m_\pi^2 + \frac{g_A^0 + g_A^{0^3}}{8\pi f_\pi^2 M_0} m_\pi^3 \\
& + \left[32F^r(\lambda) + \frac{g_A^0 + 2g_A^{0^3}}{16\pi^2 f_\pi^2 M_0^2} + \frac{g_A^0 (2 + 3g_A^{0^2})}{16\pi^2 f_\pi^2 M_0^2} \ln \frac{m_\pi}{\lambda} \right] m_\pi^4 + \mathcal{O}(m_\pi^5). \tag{39}
\end{aligned}$$

The sum of the first two terms in this expansion coincides with the leading-one-loop expression for g_A in HB χ PT, as expected in infrared regularization. The calculation gives a full tower of “recoil corrections” in the form of increasing powers of $1/M_0$. We include the counterterm $32 F m_\pi^4$ in the third-order calculation in order to achieve renormalization without neglecting recoil corrections. Since contact terms *up to and including* $\mathcal{O}(p^3)$

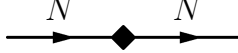


Figure 12: c_1 -insertion in a nucleon line: the diamond corresponds to the vertex $i 4 c_1 m_\pi^2$ from $\mathcal{L}_{\pi N}^{(2)}$.

cannot absorb higher-order divergences at m_π^4 , their β -functions cannot compensate for scale dependence which is suppressed by two powers of $1/M_0$. By introducing the term $32 F^r(\lambda) m_\pi^4$, we remove this unphysical scale dependence.

At order p^4 nucleon field renormalization (Fig. 4) and mass renormalization have been evaluated consistently within the accuracy in the perturbative, diagrammatic expansion at which we are working. In Fig. 12 we draw as a diamond the second order insertion in the nucleon line proportional to the low-energy constant c_1 , see Eq. (2). At order p^4 we have to compute all graphs resulting from the insertion of *at most one* c_1 -vertex in *at most one* nucleon line in the diagrams (2), (3) and (4) of Fig. 1 and in the diagram of Fig. 2. Since for small m_π

$$\frac{i}{\not{p} - (M_0 - 4 c_1 m_\pi^2)} = \frac{i}{\not{p} - M_0} + \frac{i}{\not{p} - M_0} (i 4 c_1 m_\pi^2) \frac{i}{\not{p} - M_0} + \dots, \quad (40)$$

we can summarize the c_1 -insertions by a simple shift of the pole of the nucleon propagator from the ‘‘bare’’ nucleon mass to its renormalized value at second chiral order:

$$M_N = M_0 - 4 c_1 m_\pi^2 + \mathcal{O}(p^3). \quad (41)$$

Therefore nucleon field renormalization is taken into account by

$$g_A^0 \left[1 + \frac{\partial}{\partial \not{p}} \Sigma^{(3)} \Big|_{\not{p}=M_0-4c_1m_\pi^2} + \frac{\partial}{\partial \not{p}} \Sigma^{(4)} \Big|_{\not{p}=M_0} \right]. \quad (42)$$

Here $\Sigma^{(4)}(\not{p})$ is the contribution to the nucleon self-energy from the fourth-order tadpole in Fig. 4, cf. [11],

$$\Sigma^{(4)} = \frac{3m_\pi^2 \Delta_\pi}{f_\pi^0} \left(2c_1 - \frac{p^2}{M_0^2 d} c_2 - c_3 \right). \quad (43)$$

What is relevant at order p^4 is just the linear term in the expansion of Eq. (42) in powers of c_1 .

Each of the fourth-order diagrams in Fig. 3 contributes to g_A as follows:

$$-\frac{g_A^0}{(d-1)f_\pi^2 M_0} m_\pi^2 \left[c_3 \left(\Delta_\pi + (m_\pi^2 - 4M_0^2) I_N \right) + c_4 \left(\Delta_\pi + 4(d-2)M_0^2 I_N + m_\pi^2 I_N \right) \right]. \quad (44)$$

The pion mass dependence of g_A at order p^4 is finally given by

$$\begin{aligned}
g_A = & g_A^0 + 4C^r(\lambda) m_\pi^2 + 32F^r(\lambda) m_\pi^4 + 128G^r(\lambda) m_\pi^6 - \frac{g_A^{0,3} m_\pi^2}{16\pi^2 f_\pi^2} \left[1 - \frac{32c_1 M_0^2 m_\pi^4 - 12c_1 m_\pi^6}{(4M_0^2 - m_\pi^2) M_0^3} \right] \\
& + \ln\left(\frac{m_\pi}{\lambda}\right) \frac{g_A^0 m_\pi^2}{16\pi^2 f_\pi^2} \left[-2(1 + 2g_A^{0,2}) - (3c_2 + 4c_3 - 4c_4) \frac{m_\pi^2}{M_0} + (2 + 3g_A^{0,2}) \frac{m_\pi^2}{M_0^2} \right. \\
& \left. + \frac{2}{3}(24c_1 + c_3 + c_4 + 36c_1 g_A^{0,2}) \frac{m_\pi^4}{M_0^3} \right] \\
& + \arccos\left(-\frac{m_\pi}{2M_0}\right) \frac{g_A^0 m_\pi^3}{16\pi^2 f_\pi^2 (4M_0^2 - m_\pi^2)^{3/2}} \left[-\frac{128}{3}(c_3 - 2c_4) M_0^3 \right. \\
& \left. + 32(1 + g_A^{0,2})(M_0^2 + 4c_1 M_0 m_\pi^2) + 32(c_3 - c_4) M_0 m_\pi^2 - 4(4 + 5g_A^{0,2}) m_\pi^2 \right. \\
& \left. - 8(12c_1 + c_3 + 18c_1 g_A^{0,2}) \frac{m_\pi^4}{M_0} + (2 + 3g_A^{0,2}) \frac{m_\pi^4}{M_0^2} + 2(24c_1 + c_3 + c_4 + 36c_1 g_A^{0,2}) \frac{m_\pi^6}{3M_0^3} \right] \\
& + \frac{g_A^0 m_\pi^4}{16\pi^2 f_\pi^2 M_0^3} \left[\frac{1}{12}(9c_2 + 32c_3 - 16c_4) M_0^2 - M_0 - \frac{5}{9}(c_3 + c_4) m_\pi^2 \right]
\end{aligned} \tag{45}$$

$G^r(\lambda)$ is a seventh-order effective coupling appearing in the counterterm required to absorb the divergence at m_π^6 . This compensates the unphysical scale dependence at this power in m_π . The factor 128 is motivated by the fact that the effective πN Lagrangian at order p^7 can contribute via

$$\mathcal{L}_N^{(7)} = 128 g m_\pi^6 \bar{\Psi} \frac{\tau^i}{2} a_\mu^i \gamma^\mu \gamma_5 \Psi + \dots \tag{46}$$

“Naive” dimensional arguments suggest $g = \mathcal{O}(1/\Lambda_\chi^6)$. At order p^4 one finds

$$F^r(\lambda) = F + \frac{L(\lambda)}{32f_\pi^2 M_0^2} (3g_A^{0,3} + 2g_A^0 - 3c_2 g_A^0 M_0 - 4c_3 g_A^0 M_0 + 4c_4 g_A^0 M_0) \tag{47}$$

$$G^r(\lambda) = G + \frac{L(\lambda)}{128f_\pi^2 M_0^3} (24c_1 g_A^{0,3} + 16c_1 g_A^0 + \frac{2}{3}c_3 g_A^0 + \frac{2}{3}c_4 g_A^0) . \tag{48}$$

References

- [1] The Review of Particle Physics, S. Eidelman *et al.*, Phys. Lett. **B592**, 1 (2004).
- [2] RBCK collaboration, S. Sasaki, K. Orginos, S. Ohta and T. Blum, Phys. Rev. **D68**, 054509 (2003).
- [3] LHPC collaboration, R. G. Edwards *et al.*, Phys. Rev. Lett. **96**, 052001 (2006).
- [4] QCDSF collaboration, A. Ali Khan *et al.*, [hep-lat/0603028](#).
- [5] V. Bernard, H. W. Fearing, T. R. Hemmert and U.-G. Meißner, Nucl. Phys. **A635**, 121 (1998); *Erratum ibid.* **A642**, 563 (1998).
- [6] T. R. Hemmert, M. Procura and W. Weise, Phys. Rev. **D68**, 075009 (2003).
- [7] V. Bernard and U.-G. Meissner, Phys. Lett. **B639**, 278 (2006).
- [8] T. Wollenweber, Diploma Thesis, Technische Universität München 2005.
- [9] S. R. Beane and M. J. Savage, Phys. Rev. **D70**, 074029 (2004).
- [10] J. Gasser and H. Leutwyler, Nucl. Phys. **B307**, 763 (1988).
- [11] T. Becher and H. Leutwyler, Eur. Phys. J. **C9**, 643 (1999).
- [12] M. Procura, T. R. Hemmert and W. Weise, Nucl. Phys. **A755**, 649 (2005).
- [13] M. Procura, B. U. Musch, T. R. Hemmert and W. Weise, Nucl. Phys. Proc. Suppl. **153**, 229 (2006).
- [14] M. Procura, B. U. Musch, T. R. Hemmert and W. Weise, to be published in the proceedings of the PANIC05 Conference, American Institute of Physics.
- [15] J. Kambor and M. Mojžiš, JHEP **9904**, 031 (1999).
- [16] J. Schweizer, Diploma Thesis, University of Bern (2000).
- [17] M. Procura, B. U. Musch, T. Wollenweber, T. R. Hemmert and W. Weise, Phys. Rev. **D73**, 114510 (2006).
- [18] S. Ohta *et al.*, Nucl. Phys. Proc. Suppl. **129**, 296 (2004)
Nucl. Phys. Proc. Suppl. **140**, 396 (2005) and
H. Lin, S. Ohta, [hep-lat/0610028](#).
- [19] M. Lüscher, PoS **LAT2005** (2005) 002, [arXiv:hep-lat/0509152](#).
- [20] L. Del Debbio, L. Giusti, M. Lüscher, R. Petronzio, N. Tantalo
[arXiv:hep-lat/0610059](#).

- [21] M. Göckeler, [arXiv:hep-lat/0412013](https://arxiv.org/abs/hep-lat/0412013).
- [22] S. Aoki *et al.* [JLQCD Collaboration], Phys. Rev. **D68** 054502 (2003).
- [23] V. Bernard, N. Kaiser and U.-G. Meißner, Nucl. Phys. **A615**, 483 (1997).
- [24] P. Büttiker and U.-G. Meißner, Nucl. Phys. **A668**, 97 (2000).
- [25] D. R. Entem and R. Machleidt, Phys. Rev. **C 66**, 014002 (2002).
- [26] M. Procura, T. R. Hemmert and W. Weise, Phys. Rev. **D69**, 034505 (2004).
- [27] N. Fettes, V. Bernard, U.-G. Meißner, Nucl. Phys. **A669**, 269 (2000).
- [28] N. Fettes, Berichte des Forschungszentrums Jülich Nr. 3814 (2000).
- [29] A. Manohar and H. Georgi, Nucl. Phys. **B234**, 189 (1984).
- [30] A. W. Thomas and W. Weise, *The Structure of the Nucleon*, Wiley-VCH, Berlin (2001).
- [31] S. L. Adler, Phys. Rev. Lett. **14**, 1051 (1965); S. L. Adler, Phys. Rev. **140**, B736 (1965) and *Erratum ibid.* 175, 2224 (1968); W. I. Weisberger, Phys. Rev. Lett. **14**, 1047 (1965).
- [32] S. Weinberg, Phys. Rev. Lett. **17**, 616 (1966); Y. Tomozawa, Nuovo Cimento **46A**, 707 (1966).
- [33] T. E. O. Ericson, B. Loiseau and A. W. Thomas, Phys. Rev. **C66**, 014005 (2002).
- [34] T. E. O. Ericson and W. Weise, *Pions and Nuclei*, Clarendon, Oxford (1988); G. E. Brown and W. Weise, Phys. Reports **22**, 279 (1975).
- [35] O. Hanstein, D. Drechsel and L. Tiator, Phys. Lett. **B385**, 45 (1996).
- [36] T. R. Hemmert, B. R. Holstein and J. Kambor, J. Phys. **G24**, 1831 (1998).
- [37] G. Colangelo and S. Dürr, Eur. Phys. J. **C33**, 543 (2004).
- [38] T. Appelquist and J. Carazzone, Phys. Rev. **D11**, 2856 (1975).
- [39] B. A. Ovrut and H. J. Schnitzer, Phys. Rev. **D22**, 2518 (1980).
- [40] See for example G. B. West, Found. Phys. **30**, 695 (2000).
- [41] J. A. McGovern and M. C. Birse, Phys. Lett. **B446**, 300 (1999).
- [42] J. A. McGovern and M. C. Birse, [hep-lat/0608002](https://arxiv.org/abs/hep-lat/0608002).